Calculation and analysis of cross-sections for p+^{184}W reactions up to 200 MeV *

SUN Jian-Ping(孙建平)[1]   ZHANG Zheng-Jun(张正军)[1;1)]   HAN Yin-Lu(韩银录)[2]

[1] Department of Physics, Northwest University, Xi'an 710069, China
[2] Science and Technology on Nuclear Data Laboratory, China Institute of Atomic Energy, Beijing 102413, China

Abstract: A set of optimal proton optical potential parameters for p+^{184}W reactions are obtained at incident proton energy up to 250 MeV. Based on these parameters, the reaction cross-sections, elastic scattering angular distributions, energy spectra and double differential cross sections of proton-induced reactions on ^{184}W are calculated and analyzed by using theoretical models which integrate the optical model, distorted Born wave approximation theory, intra-nuclear cascade model, exciton model, Hauser-Feshbach theory and evaporation model. The calculated results are compared with existing experimental data and good agreement is achieved.

Key words: reaction models, elastic scattering angular distribution, energy spectra, double differential cross-section

PACS: 25.10.+s, 28.20.Cz   **DOI:** 10.1088/1674-1137/39/8/084102

1   Introduction

Accelerator-driven clean nuclear power systems (ADS) are a recent topic of interest in nuclear physics, as ADS can transmute radioactive waste and produce power. Neutron sources are generated from the high energy proton bombardment of heavy nuclei and drive the subcritical reactor of ADS. The micro reaction data of intermediate and high energy reactions on heavy nuclei, such as the number of external neutron sources and their energy distribution, are the basis for the whole ADS system.

Tungsten (W) is an important target material for ADS neutron sources, and proton-induced reaction data on W in the energy range from the threshold energy to 200 MeV are necessary. In particular, data on the proton-induced energy-angle correlated spectra and double differential cross-sections of particle (neutron, proton, deuteron, triton, helium-3 and alpha-particle) emission are needed. In this paper, the cross-sections, energy spectra and double differential cross sections of p+^{184}W reactions are calculated and analyzed.

The theoretical methods and model parameters are shown in Section 2. Here the theories and methods are further improved in intermediate and high energy reactions, and then the micro data which can be used for ADS targets and other device designs are obtained from the theoretical calculations [1]. In Section 3, comparisons and analysis between the calculated results and the experimental data are given. A brief conclusion is given in Section 4.

2   Theoretical model and model parameters

The optical model [2, 3] is used to describe the experimental data of proton-induced total, non-elastic, elastic cross sections and elastic-scattering angular distributions. Furthermore, this model can be used to calculate the transmission coefficients of the compound nucleus and the pre-equilibrium emission process [4].

The optical potential is given as follows:

$$V = V_r + i(W_s + W_v) + U_{so} + V_c, \tag{1}$$

where V_r is the real part potential, W_s and W_v are the imaginary part potentials of surface absorption and volume absorption respectively, U_{so} donates the spin-orbit couple potential and V_c is the Coulomb potential.

The real part of the optical model potential is

$$V_r = -\frac{V_r(E)}{1 + \exp[(r - R_r)/a_r]}. \tag{2}$$

The imaginary part of surface absorption is

$$W_s = -4W_s(E)\frac{\exp[(r - R_s)/a_s]}{\{1 + \exp[(r - R_s)/a_s]\}^2}. \tag{3}$$

The imaginary part of volume absorption is

$$W_{\mathrm{v}} = -\frac{W_{\mathrm{v}}(E)}{1+\exp[(r-R_{\mathrm{v}})/a_{\mathrm{v}}]}. \quad (4)$$

The spin-orbit potential is

$$U_{\mathrm{so}} = -\frac{2(V_{\mathrm{so}}+\mathrm{i}W_{\mathrm{so}})}{a_{\mathrm{so}}r}\frac{\exp[(r-R_{\mathrm{so}})/a_{\mathrm{so}}]}{\{1+\exp[(r-R_{\mathrm{so}})/a_{\mathrm{so}}]\}^2}$$

$$\times [j(j+1)-l(l+1)-s(s+1)]. \quad (5)$$

The Coulomb potential is

$$V_{\mathrm{C}} = \begin{cases} \dfrac{zZe^2}{r} & \text{if } r \geqslant R_{\mathrm{C}} \\ \dfrac{zZe^2}{2R_{\mathrm{C}}}\left(3-\dfrac{r^2}{R_{\mathrm{C}}^2}\right) & \text{if } r < R_{\mathrm{C}} \end{cases}. \quad (6)$$

The potential depth of the real part $V_{\mathrm{r}}(E)$ is given as follows:

$$V_{\mathrm{r}}(E)=V_0+V_1E+V_2E^2+V_3(N-Z)/A+V_4Z/A^{1/3}, \quad (7)$$

where $W_{\mathrm{s}}(E)$ and $W_{\mathrm{v}}(E)$ represent the imaginary parts of surface and volume absorption, respectively. They can be calculated as follows:

$$W_{\mathrm{s}}(E) = \max\{0, W_{\mathrm{s}0}+W_{\mathrm{s}1}E+W_{\mathrm{s}2}(N-Z)/A\}, \quad (8)$$
$$W_{\mathrm{v}}(E) = \max\{0, W_{\mathrm{v}0}+W_{\mathrm{v}1}E+W_{\mathrm{v}2}E^2\}, \quad (9)$$

where N, Z and A are the neutron, charge and mass numbers of the target, respectively; a_{r} in Eq. (2) and a_{so} in Eq. (5) are the diffusive widths of the real part and the spin-orbit couple potential. The diffusive widths of the surface and volume absorption potential in Eqs. (3) and (4) are a_{s} and a_{v}; z represents the charge number of the incident particle; E is the proton's incident energy in the center of mass system. The spin-orbit couple potential is V_{so}.

The radii are given as follows:

$$R_{\mathrm{i}}=r_{\mathrm{i}}A^{1/3}, \; \mathrm{i}=\mathrm{r, s, v, so, c}, \quad (10)$$

where r_{r}, r_{s}, r_{v}, r_{so} and r_{c} are the radii of the real part, the surface absorption, the volume absorption, the spin-orbit couple and the Coulomb potential, respectively.

The units of the length parameters r_{r}, r_{s}, r_{v}, r_{so}, r_{c}, a_{r}, a_{so}, $a_{\mathrm{s}0}$, $a_{\mathrm{s}1}$, $a_{\mathrm{v}0}$, $a_{\mathrm{v}1}$ are in fermi (fm), the potentials V_{r}, W_{s}, W_{v}, U_{so}, V_{c} are in MeV and the energy E is also in MeV [5].

Table 1 gives the optimum proton optical model potential parameters which are obtained by using the code APMN [6] to fit the experimental data.

The code DWUCK4 [7], based on the Distorted Wave Born Approximation (DWBA), is used in this work to calculate cross-sections and angular distributions of direct inelastic scattering. The direct reaction is important in proton-induced reactions. The discrete levels of residual nuclei considered in the direct non-elastic scattering process are given in Table 2.

Table 1. Optimum proton optical model potential parameters obtained.

V_0	44.98434	r_{r}	1.26146
V_1	−0.28003	r_{s}	1.06554
V_2	0.0004	r_{v}	1.88632
V_3	−45.53588	r_{so}	1.26146
V_4	0.13797	r_{c}	1.51263
$W_{\mathrm{s}0}$	7.71606	a_{r}	0.67259
$W_{\mathrm{s}1}$	0.02640	a_{so}	0.67259
$W_{\mathrm{s}2}$	11.83579	a_{v}	0.20000
$W_{\mathrm{v}0}$	0.59395	a_{s}	0.62640
$W_{\mathrm{v}1}$	0.005150	V_{so}	6.2
$W_{\mathrm{v}2}$	−0.00076	W_{so}	0.0

Table 2. Discrete levels in direct non-elastic scattering process.

energy/MeV	$J\pi$	energy/MeV	$J\pi$
0.1112	2 +	1.3604	4 +
0.3641	4 +	1.3863	2 +
0.7483	6 +	1.4250	3 +
0.9033	2 +	1.4310	2 +
1.0060	3 +	1.4770	6 +
1.1214	2 +	1.5233	3 +
1.1338	4 +	1.5369	4 +
1.2949	5 +	1.5702	2 +

The intra-nuclear cascade model [8] can be regarded as a supplement and amendment of the direct reaction mechanism. It considers the first to fourth cascade nucleon emission process.

In the pre-equilibrium mechanism, the improved Iwamoto-Harada model [9–11] is included in the exciton model for light composite particle emissions. Zhang et al. [10, 12] improved Iwamoto et al's pick-up mechanism to reduce pre-formation probabilities. Shen [13] gave the results of a composite particle projectile considering pick-up-type reactions with one and two particles above the Fermi sea by energy-averaged and energy-angle correlated kernels, respectively. This model is used to improve the energy spectra and the double differential cross-sections in compound nucleus reactions.

Considering the restrictions of the Pauli principle, the density of excited states (p, h) of a compound nuclear system (Z, A, U) is expressed by the following formula:

$$\omega(Z,A,U,p,h)=\frac{g(gU_{\mathrm{e}})^{h'}\left[gU_{\mathrm{e}}-A(p,h)\right]^{p'-1}}{p!h!(p+h-1)!}f(U_{\mathrm{e}}). \quad (11)$$

In the above formula, if $gU_{\mathrm{e}} \leqslant A(p,h)$, then $\omega(Z,A,U,p,h)=0$. The correlation of g with excitation energy is studied and the new density of states of a single particle is proposed as follows:

$$g(U)=\frac{g_0(1-\mathrm{e}^{-U_{\mathrm{e}}\times\mathrm{ccg1}})}{U_{\mathrm{e}}\times\mathrm{ccg1}}, U_{\mathrm{e}}=U-\Delta, \quad (12)$$

where g_0 is equal to $A/13$, U is excitation energy, Δ is the energy correction and a is a parameter of level energy density.

$$f(U_e) = 0.06\pi^2/(aU_e)^{1/8}, \tag{13}$$

$$A(p,h) = \frac{1}{2}p(p-1)+\frac{1}{2}h(h-1), \tag{14}$$

$$h' = \min(p,h), \; p' = \max(p,h), \tag{15}$$

and ccg1 is set as 0.05 in our calculation.

The particle emissions are considered up to 18 times in the evaporation process. The equilibrium emissions are calculated by the evaporation model [14] for the first to eighteenth particle emissions. For the first particle emission in the low-energy region, the Hauser-Feshbach theory with the width fluctuation correction [15, 16] is also adopted.

The energy spectrum formula can be given as follows:

$$\frac{\mathrm{d}\sigma}{\mathrm{d}\varepsilon_b} = \sum_{J\pi} \sigma_a^{J\pi} \sum_n P^{J\pi}(n) \frac{W_b^{J\pi}(n,E',\varepsilon_b)}{W_T^{J\pi}(n,E')}, \tag{16}$$

where $\sigma_a^{J\pi}$ is the absorption cross-section, $W_T^{J\pi}(n,E')$ is the total emission rate at n-exciton state and $W_b^{J\pi}(n,E',\varepsilon_b)$ is the emission rate of emitted particle b with outgoing energy ε_b, E' being the excitation energy of the pre-equilibrium system. The occupation probability $P^{J\pi}(n)$ of excitation state n in the (J,π) channel is obtained by solving the J-dependent excitation master equation to conserve the angular momentum in the pre-equilibrium reaction processes. $W_T^{J\pi}(n,E')$ and $W_b^{J\pi}(n,E',\varepsilon_b)$ of particle b are given as follows:

$$W_T^{J\pi}(n,E') = \sum_b \int W_b^{J\pi}(n,E',\varepsilon_b)\mathrm{d}\varepsilon_b, \tag{17}$$

$$W_b^{J\pi}(n,E',\varepsilon_b) = \frac{2s_b+1}{\pi^2\hbar^3}\mu_b\varepsilon_b\sigma_b^{J\pi}(\varepsilon_b)\sum_{lm}F_{lm}^b(\varepsilon_b)Q_{lm}^b(n)$$
$$\times\frac{\omega(p-1,h,E'-\varepsilon_b-B_b)}{\omega(n,E')}, \tag{18}$$

where s_b and μ_b are the spin and reduced mass, $\sigma_b^{J\pi}(\varepsilon_b)$ is the inverse cross-section of the b particle, $F_{lm}^b(\varepsilon_b)$ stands for the formation factor of the emitted particle b with the configuration $[l,m]$ from the pick-up mechanism of the improved Iwamoto-Harade model, and $F_{lm}^b(\varepsilon_b)=1$ for nucleons and for light composite particles (deuteron, triton, helium and alpha-particle) [10, 12]. The configuration $[l,m]$ is composed of l particles above the Fermi level and m particles below. $Q_{lm}^b(n)$ is a combination factor to account for nucleon types that composed the cluster for memory by the excitation system, p and h are numbers of particles and holes, $n=p+h$ and $\omega(n,E')$ is the exciton state density. The explicit expressions for $F_{lm}^b(\varepsilon_b)$, $Q_{lm}^b(n)$ and $\omega(n,E')$ can be found in Ref. [10].

The double differential cross-sections are provided by the equation

$$\frac{\mathrm{d}^2\sigma}{\mathrm{d}\Omega\mathrm{d}\varepsilon_b} = \frac{1}{4\pi}\left(\frac{\mathrm{d}\sigma^{PE}}{\mathrm{d}\varepsilon_b}+\frac{\mathrm{d}\sigma^{EQ}}{\mathrm{d}\varepsilon_b}\right)\frac{a}{\sinh(a)}$$
$$\times[\cosh(a\cos\theta)+f_{PE}\cdot\sinh(a\cos\theta)], \tag{19}$$

where θ is the emission angle in the center of mass frame and a is the slope parameter depending on the incident particle type and energy, the target nucleus and the emitting channel. It can be calculated using the procedure in Ref. [17]. The f_{PE} parameter is the fraction of particle emission apart from the equilibration process. It can be calculated as follows:

$$f_{PE} = \frac{(\mathrm{d}\sigma/\mathrm{d}\varepsilon_b)_{PE}}{(\mathrm{d}\sigma/\mathrm{d}\varepsilon_b)_{PE}+(\mathrm{d}\sigma/\mathrm{d}\varepsilon_b)_{EQ}}, \tag{20}$$

where PE and EQ stand for the pre-equilibrium emission and equilibrium emission respectively. The double differential cross-sections can be calculated by the above energy spectra.

All reaction cross-sections for protons on ^{184}W are studied using the optical model theory at energy up to 500 MeV. Credible optical model potential parameters for total reaction cross section and main reaction channels are obtained; they are used as input parameters to the code MEND [18] to calculate the direct reaction cross section, pre-equilibrium and equilibrium emission.

3   Results and analysis

In Fig. 1, the calculated fission cross sections of p+^{184}W, ^{208}Pb, ^{209}Bi and ^{202}Hg reactions are given and compared with experimental data (here, we use the energy density theory that adopts the Gilbert-Cameron formula and the fission cross section formulas [19–22]). These experimental data for fission cross sections for the proton-induced ^{208}Pb and ^{209}Bi reactions are cited from Ref. [23], while no experimental data for ^{184}W and ^{202}Hg reactions are found. We can obviously observe that the fission cross section decreases quickly with the decreasing of proton number Z and mass number A of the target nucleus. The fission cross section for p+^{184}W is only 30 mb at energy 300 MeV. This is less than 2% of the reaction cross section.

The calculated results of proton reaction cross-sections for ^{184}W and the experimental data for ^{nat}W [24] are shown in Fig. 2. There are no experimental data for the p+^{184}W reaction. The calculated results of proton reaction cross-sections for ^{184}W are in good agreement with the experimental data of natural W. The calculated proton cross-sections are compared with experimental data [24–26] for the p+^{181}Ta reaction in Fig. 2 and the theoretical results are consistent with these experimental data.
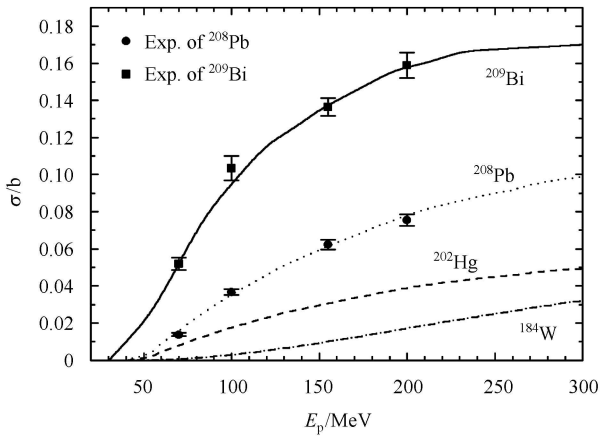
Fig. 1. Calculated fission cross sections (lines) are compared with experimental data (points) of p+^{208}Pb and ^{209}Bi reactions. The theoretical results for p+^{202}Hg and ^{184}W reactions are given without experimental data.
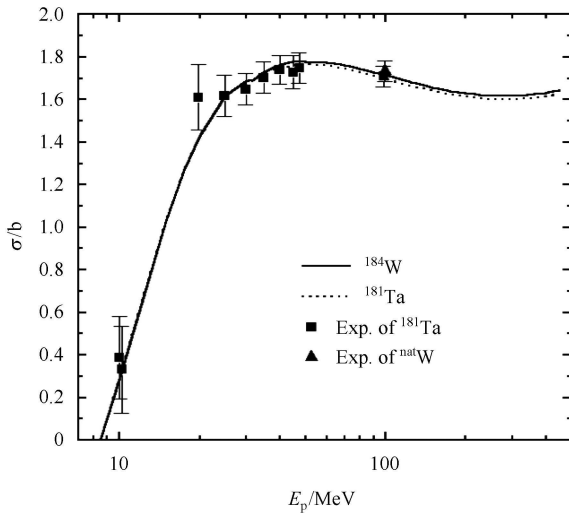

Fig. 2. Proton reaction cross-sections for the p+^{184}W reaction (calculated: solid line, experimental data: triangles) and p+^{181}Ta reaction (calculated: dotted line, experimental data: squares).

A comparison of the calculated results and relevant experimental data for elastic scattering angular distributions for p+^{184}W and p+^{181}Ta reactions are shown in Fig. 3. The experimental data of p+^{181}Ta at energies of 146 MeV and 340 MeV are from Refs. [27, 28] and the data for the p+^{nat}W reaction at 340 MeV are from Ref. [28]. The calculated results agree with experimental data well, except for the theoretical results for ^{184}W at lower angles, which are smaller than the experimental data.

The optical model potential parameters of ^{184}W are proved credible from Fig. 2 and Fig. 3, so this set of

optical model potential parameters will be adopted in the following calculations. The results reproduce the experimental data well, and the optical model potential parameters can be used in the vicinity of W nuclei.
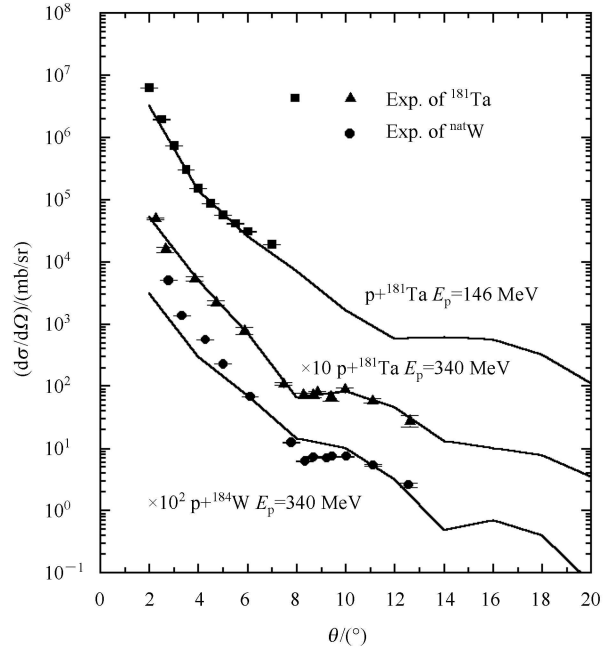

Fig. 3. Calculated proton elastic scattering angular distribution (solid lines) are compared with experimental data (points) for p+^{181}Ta and p+^{184}W reactions at different energies.

The calculated cross-sections for ^{184}W (p, kn) reaction channels (where k is set as 1, 2, 3, 4, 5, 6, 7, 8 and 9) are shown in Fig. 4. There are no experimental data for the ^{184}W (p, kn) reaction channels. The calculated results for the ^{184}W (p, pkn) reaction cross-sections are given in Fig. 5. We can see that the number of neutrons emitted changes as the proton-induced energy increases. Furthermore, the competition mechanism between the different reaction channels is obvious. As shown in Figs.4–5, the cross section value firstly increases as the energy increases, and then it decreases. When the (n, kn) channel cross section starts to reduce, at the same time, the [n, (k+1)n] reaction channel opens. This is reasonable, and supports our calculated results.

Table 3. Long-lived radioactive products from the p+^{184}W reaction.

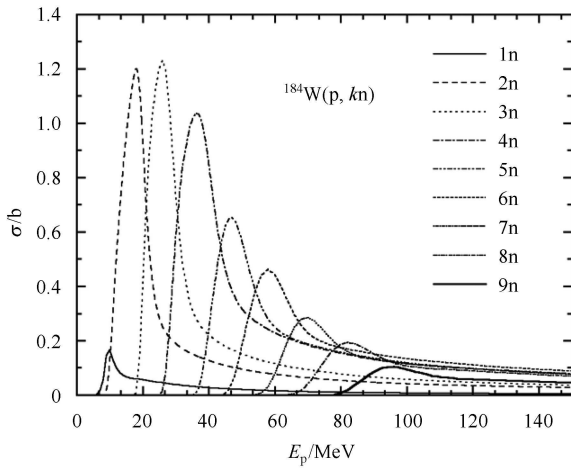| residual nuclei	channels	half-life/year
^{183}W	^{184}W(p, x)^{183}W	1.1×10^{17}
^{180}Ta	^{184}W(p, x)^{180}Ta	1.2×10^{15}
^{179}Ta	^{184}W(p, x)^{179}Ta	1.82
^{182}Hf	^{184}W(p, x)^{182}Hf	9×10^{6}
^{178}Hf	^{184}W(p, x)^{178}Hf	31
^{174}Hf	^{184}W(p, x)^{174}Hf	2×10^{15}
^{172}Hf	^{184}W(p, x)^{172}Hf	1.87

Fig. 4.   Calculated reaction cross-sections for ^{184}W (p, kn) channels, where k=1, 2, 3, 4, 5, 6, 7, 8, 9.
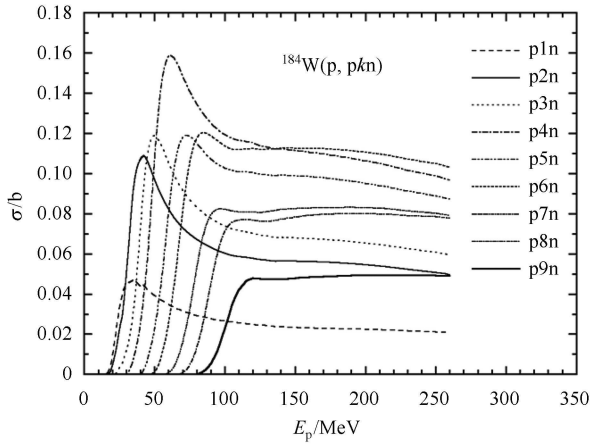

Fig. 5.   Calculated cross-sections for ^{184}W (p, pkn) reaction channels, where k=1, 2, 3, 4, 5, 6, 7, 8, 9.

Long-lived radioactive reaction products from the p+^{184}W reactions whose half-lives are greater than one year and cross-section values are larger than 1 mb are shown in Table 3. The cross-sections calculated are shown in Fig. 6.

The energy spectra and double differential cross sections of emission neutron, proton, deuteron, triton, helium and alpha particle for p+^{184}W reactions are also calculated. The calculated energy spectra of the neutron emission for p+^{184}W at incident proton energies of 50, 100, 150, 200 and 250 MeV are shown in Fig. 7. We can find that the shapes of calculated energy spectra for neutron emission are similar at the various energies. The calculation results show the contributions to the energy spectra are mainly the evaporation model below the neutron emission energy of 15.0 MeV and the pre-equilibrium process above 15.0 MeV.
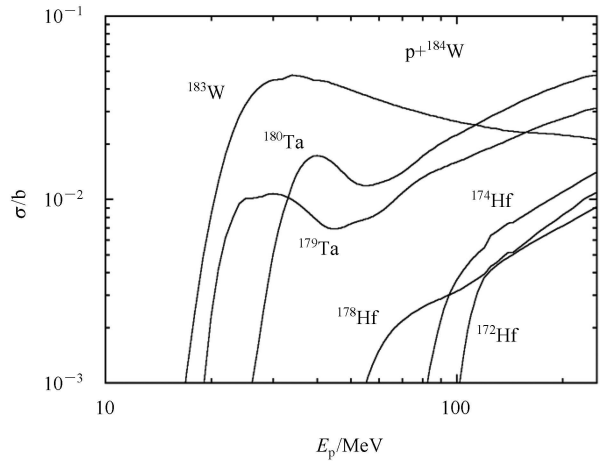

Fig. 6.   Cross sections of long-lived radioactive reaction products from the p+^{184}W reactions.

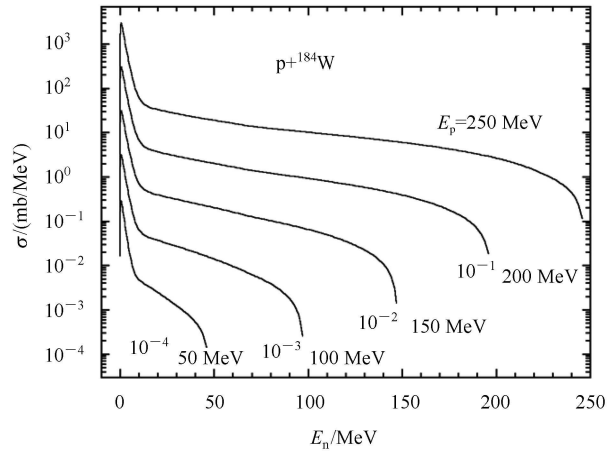

Fig. 7.   Theoretical energy spectra of neutron emission for the p+^{184}W reaction.
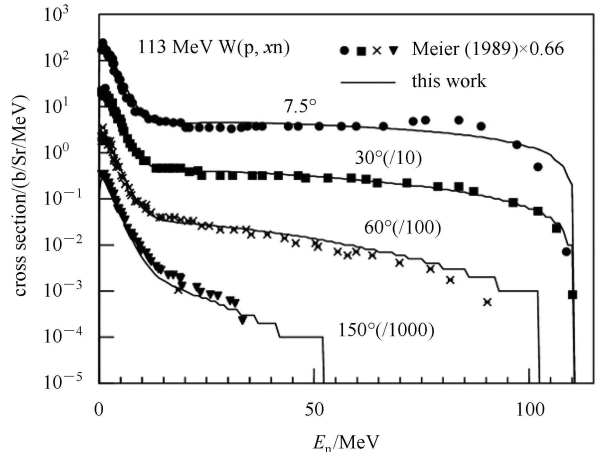

Fig. 8.   Calculated double differential cross section of neutron emission (solid line) compared with experimental data (symbols) in p+^{184}W reaction at 113 MeV incident energy at 7.5, 30.0, 60.0 and 150.0°.
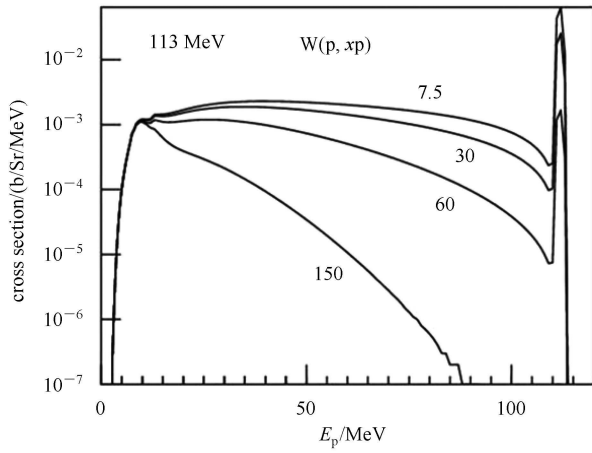
Fig. 9.   Double differential cross sections of proton emission for p+^{184}W reactions calculated at 113.0 MeV incident energy.

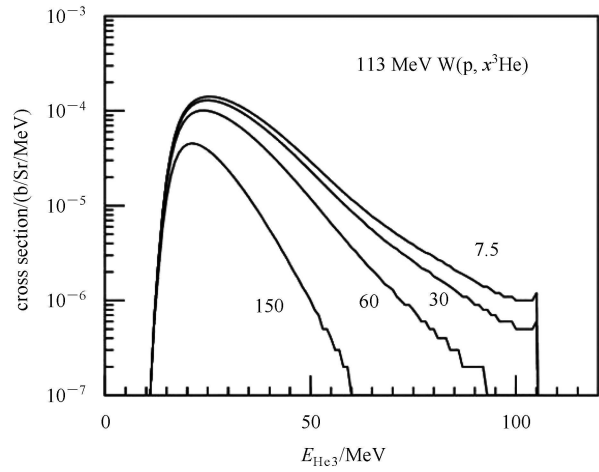Fig. 10.   Double differential cross sections of deuteron emission in p+^{184}W reactions calculated at energy 113.0 MeV.
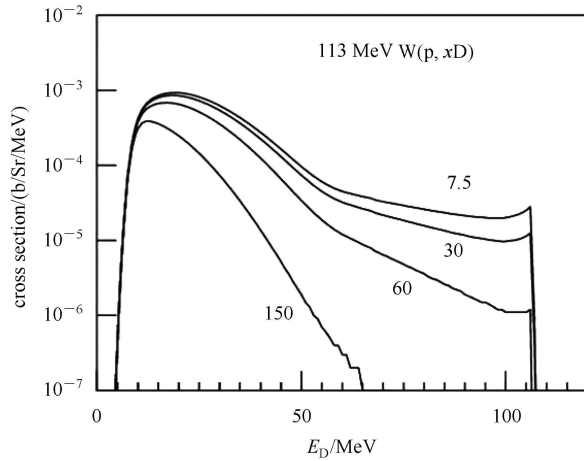

Fig. 11.   Calculated double differential cross sections of triton emission in p+^{184}W reactions calculated at energy 113.0 MeV.

Fig. 12.   Double differential cross sections of helium-3 emission in p+^{184}W reactions calculated at energy 113.0 MeV.
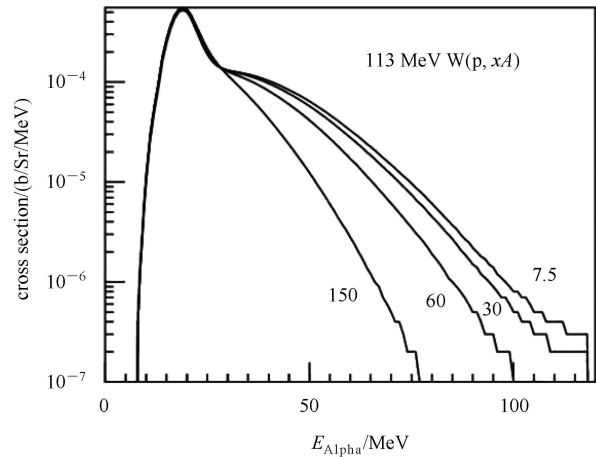

Fig. 13.   Double differential cross sections of alpha-particle emission in p+^{184}W reactions calculated at energy 113.0 MeV.
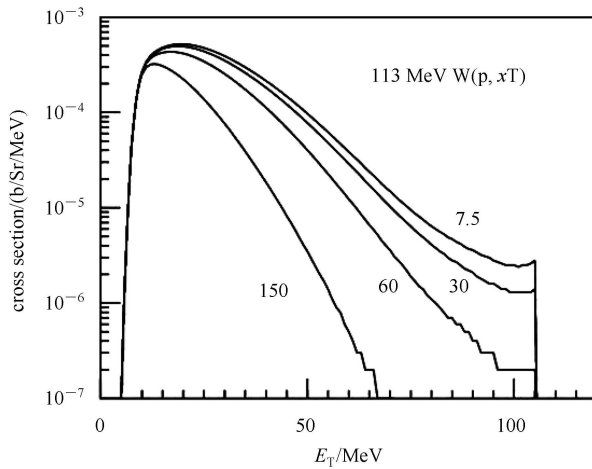
The calculated double differential cross sections of neutron emission and the experimental data taken from Ref. [29] at an incident proton energy of 113.0 MeV are given in Fig. 8. The original experimental data are multiplied by 0.66 for the processing problem [30]. From Fig. 8, the calculated results are in good agreement with experimental data at emission angles 7.5, 30.0, 60.0 and 150.0°. There are no experimental data at other energies for double differential cross sections of neutron emission. There are no experimental data for double differential cross sections of proton, deuteron, triton, helium and alpha emission for p+^{184}W reactions.

The double differential cross sections of proton emission at energy 113.0 MeV are shown in Fig. 9. The peaks of the curves at high proton emission energy

are contributed from the direct reaction mechanism. We can observe from this chart that the spectra at large angles become softer. It indicates that the pre-equilibrium mechanism contribution is dominant at high energy.

The calculated results of the double differential cross sections of deuteron, triton, helium and alpha particle emissions for p+^{184}W reactions at proton incident energy 113.0 MeV are given in Figs. 10–13. The calculated scattering angles are 7.5, 30.0, 60.0 and 150.0^o. Although there are no experimental data, we deduce that the calculated double differential cross sections are still applicable, for the shapes of these curves at different scattering angles are similar to each other. Further accurate experimental data are needed in the future.

4   Conclusions

A set of suitable proton optical potential parameters are obtained for p+^{184}W reactions at an incident proton energy up to 250 MeV, based on the corresponding experimental data of non-elastic cross-sections and elastic scattering angular distributions. The theoretical models used in this calculation, including the optical model, intra-nuclear cascade model, distorted Born wave approximation theory, pre-equilibrium and equilibrium reaction theories, provide good descriptions of the shape and magnitude of the energy spectra and double differential cross sections of proton, neutron, deuteron, triton, helium and alpha particle emissions. The calculated results are valuable for the design of ADS and other practical applications.

References

1   HAN Yin-Lu, ZHANG Yue, GUO Hai-Rui. Nuclear Instruments and Methods in Physics Research B, 2007, **265**: 461
2   Woods R D, Saxon D S. Phys. Rev., 1954, **95**: 577
3   Becchetti F D, Jr., Greenless G W. Phys. Rev., 1969, **182**: 1190
4   HOU Pei-You, SUN Xiao-Jun, YU Cheng-Gang et al. Chinese Physics C, 2011, **35**(1): 35
5   REN Wen-Tao, ZHANG Zheng-Jun, HAN Yin-Lu. Nuclear Instruments and Methods in Physics Research B, 2011, **269**: 472
6   SHEN Qing-Biao. Nucl. Sci. Eng., 2003, **143**: 202
7   Kunz P D. Distorted Wave Code DWUCK4. Boulder, Colorado: University of Colorado, 1994
8   CHEN K, Fraenkel Z, Friedlander G et al. Phys. Rev., 1968, **166**: 949
9   Griffin J J. Phys. Rev. Lett., 1966, **17**: 478
10 ZHANG Jing-Shang, YAN Shi-Wei, WANG Cui-Lan. Z. Phys. A, 1992, **344**: 251
11 Iwamoto A, Harada K. Phys. Rev. C, 1982, **26**: 1821
12 ZHANG Jing-Shang. Nucl. Sci. Eng., 1994, **116**: 35
13 SHEN Qing-Biao. Nucl. Sci. Eng., 1994, **117**: 99
14 Weisskopf V. Phys. Rev., 1937, **52**: 295
15 Mantzouranis G, Weidenmuller H, Gassi D A. Z. Phys. A, 1976, **276**: 145
16 SUN Zhi-Qing, WANG Shu-Nuan, ZHANG Jing-Shang et al. Z. Phys. A, 1982, **305**: 61
17 Kalbach C. Physical Review C, 2005, **71**: 034606
18 CAI Chong-Hai. Nucl. Sci. Eng., 2006, **153**: 93
19 FENG Ren-Fa, WU Xi-Zhen, ZHUO Yi-Zhong. High Energy Phys. and Nucl. Phys., 1994, **18**: 361
20 Gilbert A, Cameron A G W. Can. J. Phys., 1965, **43**: 1446
21 SU Zong-Di, WANG Cui-Lan, ZHUANG You-Xiang et al. A New Set of Level Density Parameters from Feimi Gas Model. Report INDC(CPR)-2, IAEA, Vienna, 1985. 11–13
22 Ignatyuk A V, Smirenkin G N, Tishin A S. Sov. J. Nucl. Phys., 1975, **21**: 255
23 Shigaev O E, Bychenkov V S, Lomanov M F et al. The Definition of Anisotropy and Fission Cross Sections as a Function of Z**2/A at the Proton Energy 200 MeV. R, RI, 1973. 17
24 Kirkby P, Link W T. Can. J. Phys., 1966, **44**: 1847
25 Abegg R, Birchall J, Davison N E et al. Nuclear Physics A, 1979, **324**: 109
26 Wilkins B D, IGO G. Physical Review, 1963, **129**: 2198
27 Steinberg D J, Palmieri J N, Cormack A M. Nuclear Physics, 1964, **56**: 46
28 Richardson R E, Ball W P, Leith C E et al. Physical Review, 1952, **86**: 29
29 Meier M M, Clark D A, Goulding C A et al. Nuclear Science and Engineering, 1989, **102**: 310
30 Chadwick M B, Young P G, Chiba S et al. Nuclear Science and Engineering, 1999, **131**: 293